

Nonequilibrium calcium dynamics optimizes the energetic efficiency of mitochondrial metabolism

Valérie Voorluijs^{a,b,1}, Francesco Avanzini^{a,1}, Gianmaria Falasco^{a,c,1}, Massimiliano Esposito^{a,1}, and Alexander Skupin^{a,b,d,1}

^aComplex Systems and Statistical Mechanics, Department of Physics and Materials Science, University of Luxembourg, L-1511 Luxembourg, Luxembourg.; ^bLuxembourg Centre for Systems Biomedicine, University of Luxembourg, L-4365 Esch-sur-Alzette, Luxembourg.; ^cDepartment of Physics and Astronomy, University of Padova, Via Marzolo 8, I-35131 Padova, Italy.; ^dDepartment of Neuroscience, University of California San Diego, CA 92093, USA.

This manuscript was compiled on March 17, 2023

Living organisms continuously harness energy to perform complex functions for their adaptation and survival while part of that energy is dissipated in the form of heat or chemical waste. Determining the energetic cost and the efficiency of specific cellular processes remains a largely open problem. Here, we analyze the efficiency of mitochondrial adenosine triphosphate (ATP) production through the tricarboxylic acid (TCA) cycle and oxidative phosphorylation that generates most of the cellular chemical energy in eukaryotes. The regulation of this pathway by calcium signaling represents a well-characterized example of a regulatory cross-talk that can affect the energetic output of a metabolic pathway, but its concrete energetic impact remains elusive. On the one hand, calcium enhances ATP production by activating key enzymes of the TCA cycle, but on the other hand calcium homeostasis depends on ATP availability. To evaluate how calcium signaling impacts the efficiency of mitochondrial metabolism, we propose a detailed kinetic model describing the calcium-mitochondria cross-talk and we analyze it using a nonequilibrium thermodynamic approach: after identifying the effective reactions driving mitochondrial metabolism out of equilibrium, we quantify the thermodynamic efficiency of the metabolic machinery for different physiological conditions. We find that calcium oscillations increase the efficiency with a maximum close to substrate-limited conditions, suggesting a compensatory effect of calcium signaling on the energetics of mitochondrial metabolism.

calcium signaling | metabolism | nonequilibrium thermodynamics | energetic cost

Life relies on permanent conversions between different forms of energy, a phenomenon referred to as energy transduction. A wide range of cellular processes are fueled by the chemical energy stored in adenosine triphosphate (ATP), but the compartmentalization of eukaryotic cells also enables the storage of potential energy across the membranes of organelles (1). Energy transduction is mediated by enzymes and pumps driven in a nonequilibrium thermodynamic manner by the hydrolysis of ATP, chemical gradients or membrane potentials.

In optimal scenarios where transduction is fully efficient, the input energy is completely transformed into usable work. However, biological processes are typically accompanied by entropy production, *i.e.*, dissipation of energy in the form of heat and/or chemical waste that is unusable for transduction (2). For example, the action of many transmembrane ionic pumps transporting ions against their concentration gradient is often based on catalysing the hydrolysis of ATP. The chemical energy released by hydrolysis is partly used to drive ionic transport while another part is dissipated. In the extreme case of pump uncoupling, also known as “slippage”, all the energy of ATP hydrolysis is dissipated without any ion transport (3).

Different nonequilibrium kinetic models have been developed to account for energy loss in pumps (4–7) but have only provided limited insights into energetic costs at the pathway level. New approaches based on metabolic network reconstruction and nonequilibrium thermodynamics are gradually emerging to rationalize the energetic costs of cellular processes (8) including gene regulation (9), repair mechanisms (10, 11), enzymatic catalysis (12), information processing (13) or signaling (14, 15). A framework to study energy transduction in complex open chemical reaction networks (CRN) has recently been proposed and used to study the efficiency of pathways of the central energy metabolism in the absence of regulations (16). Evaluating the efficiency of tightly coupled transduction processes, *i.e.* processes whose input and output currents are equal, is straightforward as it does not depend on the net reaction flux. However, when regulations come into play, this tight coupling can be lost and kinetic models become indispensable to evaluate the flux of the different processes contributing to the efficiency.

Here, we resort to a such a kinetically-detailed nonequilibrium thermodynamic approach to show and quantify how active signaling can have a beneficial energetic impact on metabolism. In particular, we analyze the efficiency of the mitochondrial production of ATP *via* the tricarboxylic acid (TCA) cycle and oxidative phosphorylation (OXPHOS), and

Significance Statement

Mitochondria are crucial to cellular energy management and impairments in mitochondrial energy metabolism are linked to a variety of pathologies including neurodegeneration, diabetes and cancer. Homeostasis of mitochondrial metabolism is regulated by diverse active processes to maintain cells in a favorable energy state, where calcium signaling is a predominant mechanism. The cross-talk between calcium dynamics and mitochondrial metabolism is based on the energy-dependent intracellular calcium management and the activating action of calcium on mitochondrial energy production. Here we show that this essential regulatory interplay exhibits robustly a maximal efficiency at the onset of calcium oscillations which maximizes ATP production and therefore represents an essential regulation of cell maintenance.

Author contributions: A.S., M.E., V.V., F.A. and G.F. designed research; V.V., F.A., G.F., A.S. and M.E. performed research; V.V., F.A., G.F., A.S. and M.E. analyzed data; and V.V., A.S., F.A., G.F. and M.E. wrote the paper.

The authors declare no conflicts of interest.

¹To whom correspondence should be addressed. E-mail: valerie.voorluijs@uni.lu, francesco.avanzini@uni.lu, gianmaria.falasco@unipd.it, massimiliano.esposito@uni.lu, alexander.skupin@uni.lu

take into account its regulation by calcium (Ca^{2+}). Since intracellular Ca^{2+} dynamics is strongly nonlinear (which can lead to oscillations in Ca^{2+} concentration) and depends itself on ATP availability, evaluating the net effect of signaling on the energetic efficiency of mitochondria is not straightforward. Our analysis quantifies the energetic efficiency of this essential cellular process beyond steady-state conditions, such as in an oscillatory regime. Overall, the proposed framework is laying the foundations for a more comprehensive characterization of energetic costs in biology.

Biological background

In mitochondria, Ca^{2+} activates two key enzymes of the TCA cycle (isocitrate dehydrogenase and α -ketoglutarate dehydrogenase) (17–20) and thereby increases the flux of high energy electrons, in the form of NADH, feeding the electron transport chain. The successive redox reactions in the mitochondrial membrane contribute to the establishment of the proton motive force driving the mitochondrial synthesis of ATP by F1F0-ATPase. Depending on the concentration of cytosolic ATP, Ca^{2+} can, however, be sequestered into cell compartments other than mitochondria, such as the endoplasmic reticulum (ER) *via* the sarcoendoplasmic reticulum Ca^{2+} ATPase (SERCA), or extruded to the extracellular space (21). These mechanisms ensure that Ca^{2+} does not accumulate in the cytosol, as a persistent high cytosolic Ca^{2+} concentration is toxic for the cell. The central coupling enabling the Ca^{2+} -mitochondria cross-talk is thus given by the Ca^{2+} fluxes between the cytosol and the ER or mitochondria (Fig. 1). The Ca^{2+} release from the ER, by leakage or *via* channels (IP₃Rs) upon stimulation by inositol 1,4,5-trisphosphate (IP₃), and Ca^{2+} exchanges with mitochondria are ATP-independent, as opposed to Ca^{2+} transport into the ER that relies on ATP-consuming SERCA pumps.

Modeling and theoretical frameworks

We developed a curated model for the essential Ca^{2+} -metabolism system integrating different modules (22–31). Its comprehensive parameterization on experimental data represent a major step towards the detailed analysis of the mitochondrial regulation by Ca^{2+} . The underlying kinetic models originally aimed at capturing the essential mechanisms of the Ca^{2+} -metabolism interplay and at rationalizing experimental data about the response of Ca^{2+} signals to changes in mitochondrial activity (and *vice versa*). After refining these models to combine them in a coherent way, we analyzed the coupled pathways by a nonequilibrium thermodynamic description of CRN (16, 32–37).

To compute their metabolic efficiency, we analyzed mitochondria as out-of-equilibrium chemical engines (Fig. 1B) satisfying the second law of thermodynamics (33, 36):

$$T\sigma = -d_t\mathcal{G} + \dot{w}_{nc} + \dot{w}_{driv}. \quad [1]$$

Mitochondrial metabolism constitutes an open CRN that continuously harnesses the free energy stored in buffered species (e.g., AcCoA, CoQ, O₂, H_m⁺) to synthesize ATP_c from ADP_c while being influenced by Na⁺ homeostasis and cytosolic processes such as Ca^{2+} signaling and ATP_c consumption. From a thermodynamic perspective, the synthesis of ATP_c and the regulations correspond to free energy exchanges between the

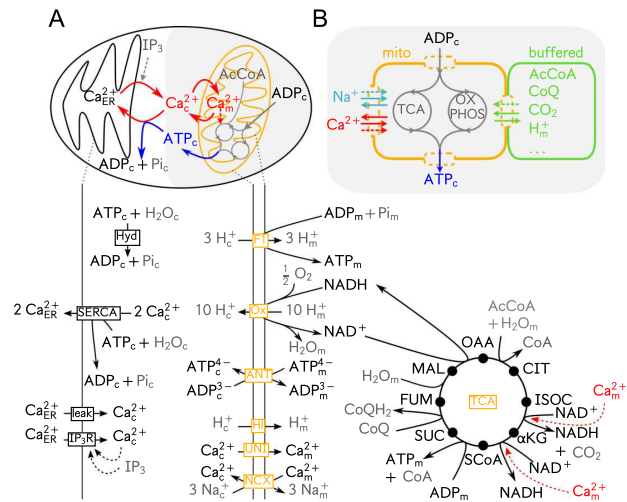


Fig. 1. Representation of the model components, conceptualization of mitochondria as a chemical engine and corresponding abbreviations. Balanced chemical equations, detailed expressions of the reaction rates, thermodynamic forces and reference parameter values are given in Tables S1, S2, S3 and S4 in S1 Appendix, respectively. (A) The upper part depicts the Ca^{2+} (red) and ATP (blue) fluxes responsible for the cross-talk between Ca^{2+} dynamics and mitochondrial metabolism. The bottom part is a detailed description of the model components. The kinetic rates for TCA cycle fluxes and processes involving exchanges across the mitochondrial membrane are respectively originating from Dudycha (22) and Magnus-Keizer models (23–25), except for the transformation of MAL into OAA, which is described more realistically by a reversible flux (26). Here, OXPHOS corresponds to the net redox reaction resulting from the electron transport chain (Ox) and the synthesis of ATP by the F1F0-ATPase (F1). A last module, consisting of Ca^{2+} exchanges across the ER membrane and cytosolic ATP hydrolysis are taken from the models from Komin *et al.* (27) and from Wacquier *et al.* (28). Controlled species (*i.e.*, species whose concentration is assumed to be constant) are shown in gray, dynamical species in black and dashed arrows represent regulations. Processes are annotated in yellow and black boxes for mitochondrial and cytosolic/ER processes, respectively. (B) Mitochondrial metabolism is conceptualized as an open chemical engine that transforms ADP_c into ATP_c through a set of 2 emergent cycles split in 3 effective reactions. Some of the controlled species involved in the internal reactions are buffered at a constant concentrations (green), while Na⁺ (turquoise) and Ca^{2+} (red) regulate reaction rates by activating specific enzymes or acting on the mitochondrial membrane potential. Abbreviations: AcCoA – acetyl coenzyme A, α KG – alpha-ketoglutarate, ATP – Adenosine triphosphate, ADP – Adenosine diphosphate, CIT – citrate, CoA – coenzyme A, CoQ/CoQH₂ – coenzyme Q10, FUM – fumarate, IP₃ – inositol 1,4,5-trisphosphate, ISOC – isocitrate, MAL – malate, NAD⁺/NADH – nicotinamide adenine dinucleotide, OAA – oxaloacetate, Pi – inorganic phosphate, SUC – succinate, SCoA – succinyl coenzyme A.

mitochondrial engine and its surroundings. They appear in the second law (Eq. 1) as the nonconservative work rate, \dot{w}_{nc} , and the driving work rate, \dot{w}_{driv} , respectively. The difference between their sum and the variation in time of the internal Gibbs free energy of mitochondria, \mathcal{G} , equals the free energy dissipated by the mitochondrial reactions, *i.e.* the entropy production rate (EPR) σ times the absolute temperature T .

The expressions of the thermodynamic quantities in Eq. 1 are derived for mitochondrial metabolism using a topological analysis (developed in refs. (35, 36)) of the corresponding CRN, which allowed us to identify conservation laws and emergent cycles. The conservation laws define parts of molecules that remain intact in all mitochondrial reactions and are instrumental to determine the Gibbs free energy \mathcal{G} . The emergent cycles define the 3 effective reactions in Eqs. 2–4 and split the nonconservative work rate into the sum of 3 contributions:

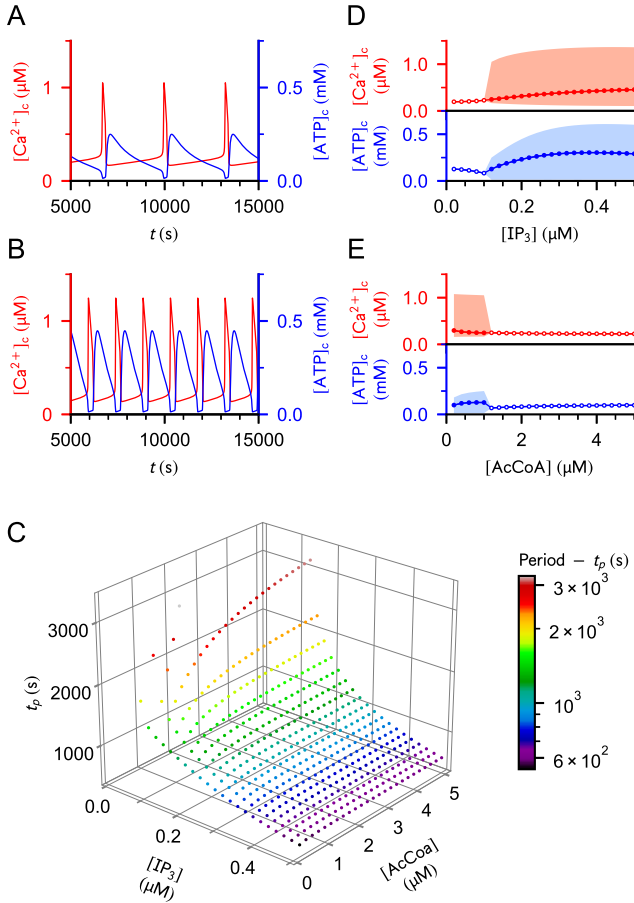
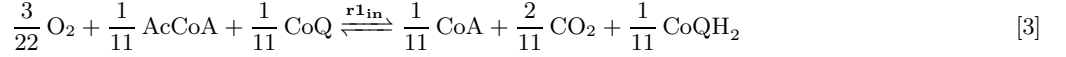


Fig. 2. Kinetic behavior of the system. (A-B) Ca_c^{2+} and ATP_c concentrations over time for $[\text{AcCoA}] = 1 \mu\text{M}$ and (A) $[\text{IP}_3] = 0.12 \mu\text{M}$ or (B) $[\text{IP}_3] = 0.20 \mu\text{M}$. (C) Effect of $[\text{IP}_3]$ and $[\text{AcCoA}]$ on the oscillation period. (D-E) Average concentration of Ca_c^{2+} and ATP_c as a function of (D) $[\text{IP}_3]$ for $[\text{AcCoA}] = 1 \mu\text{M}$ or as a function of (E) $[\text{AcCoA}]$ for $[\text{IP}_3] = 0.12 \mu\text{M}$. Empty and filled dots represent steady-state and oscillatory regimes, respectively, and the boundaries of the shaded areas correspond to the minimum and maximum concentrations. Parameter values are given in Table S4 of SI Appendix. Fig. S1B illustrates the behavior of $[\text{ATP}]_c$ for an extended range of $[\text{AcCoA}]$ and $[\text{IP}_3]$.

$\dot{w}_{\text{nc}} = \dot{w}_{r_{1,\text{out}}} + \dot{w}_{r_{1,\text{in}}} + \dot{w}_{r_2}$, where $\dot{w}_{r_{1,\text{out}}}$ quantifies the mitochondrial free energy output corresponding to the synthesis of ATP in the cytosol (Eq. 2), while $\dot{w}_{r_{1,\text{in}}}$ and \dot{w}_{r_2} quantify the mitochondrial free energy power source due the interconversion of the buffered species *via* reactions in Eqs. 3 and 4, respectively.

The average thermodynamic efficiency $\bar{\eta}$ of mitochondria can then be calculated as

$$\bar{\eta} = -\frac{\bar{w}_{\text{nc}}^{\text{output}}}{\bar{w}_{\text{nc}}^{\text{input}} + \bar{w}_{\text{driv}}} \quad [5]$$

where $\bar{w}_{\text{nc}}^{\text{input}} = \bar{w}_{r_{1,\text{in}}} + \bar{w}_{r_2}$ and $\bar{w}_{\text{nc}}^{\text{output}} = \bar{w}_{r_{1,\text{out}}}$, and the overline denotes either steady-state quantities or averages over one period of Ca^{2+} oscillations (notice that $\overline{d_t \mathcal{G}} = 0$).

The EPR nonconservative and driving work contributions vanish at equilibrium according to the second law of thermodynamics but take finite values in nonequilibrium regimes (Fig. 3B). The nonequilibrium kinetics of the system was assessed for different stimulation conditions and mitochondrial substrate concentrations (*i.e.* for different $[\text{IP}_3]$ and $[\text{AcCoA}]$ in the simulations), which allowed the calculation of the corresponding nonconservative and driving work contributions and, ultimately, of the efficiency of mitochondrial metabolism.

Results

Ca^{2+} -metabolism cross-talk affects the oscillation period and the production of ATP. To validate the kinetic model, we compared our simulation results to experimental and simulation data from the literature. Slow spiking is found around the bifurcation point corresponding to the transition from steady-state to oscillations, which marks the onset of the signaling machinery. A decrease in the oscillation period is observed as $[\text{IP}_3]$ is increased (Fig. 2A-C) or as $[\text{AcCoA}]$ is decreased (Fig. 2C). These trends are in agreement with stimulation experiments performed in various cell types (38–42) and with behaviors reported for limited availability of mitochondrial substrate (28, 42, 43). In the oscillatory regime, $[\text{ATP}]_c$ displays a maximum in dependence on $[\text{IP}_3]$ and $[\text{AcCoA}]$, a feature that is also predicted by the model of Wacquier *et al.* (28). In our simulations, a cusp in the average of $[\text{ATP}]_c$ is additionally observed at the critical point (Fig. 2D-E).

Most of these observations can be rationalized based on the dependence of SERCA pumps on ATP_c , which enables the switch between ER and mitochondrial Ca^{2+} sequestration and is a key signature of the Ca^{2+} -metabolism cross-talk. As $[\text{IP}_3]$ increases, more Ca^{2+} is released into the cytosol through IP_3Rs . The steady-state $[\text{ATP}]_c$ thus decreases due to a more demanding maintenance of the basal $[\text{Ca}^{2+}]_c$ *via* SERCA pumps. At the critical $[\text{IP}_3]$ corresponding to the onset of oscillations, mitochondrial sequestration of Ca^{2+} becomes significant, which not only relieves SERCA pumps but also enables the activation of Ca^{2+} -sensitive dehydrogenases of the TCA cycle (Fig. S2). These combined effects result in an increase of the average $[\text{ATP}]_c$. Increasing $[\text{IP}_3]$ further leads to saturation in mitochondrial buffering of Ca^{2+} (Fig. S2). More intense Ca^{2+} sequestration *via* SERCA pumps is then required and the associated ATP_c consumption is no longer counterbalanced by the Ca^{2+} -enhanced mitochondrial activity, which results in a slow decrease in average $[\text{ATP}]_c$. Meanwhile, increasing stimulation by IP_3 favors more frequent opening of the IP_3Rs , which results in an increase of the oscillation period. In most mathematical models for Ca^{2+} signaling and in agreement with experimental observations, the oscillation pe-

riod saturates at high $[IP_3]$ (44) and, beyond a critical $[IP_3]$, oscillations disappear. The cell then exhibits a high- $[Ca^{2+}]_c$ steady-state (39), as reproduced by our simulations (Fig. S2). Further stimulation by IP_3 does not affect the steady-state concentrations reached after termination of the oscillations (see Fig. 3C bottom for $[ATP]_c$ and Fig. S2 for $[Ca^{2+}]_c$ and $[Ca^{2+}]_m$), suggesting that IP_3 R s have reached their maximal release rate and contribute to saturation effect.

The impact of AcCoA level on $[ATP]_c$ and oscillation period is more visible in starving conditions, *i.e.* $[AcCoA] \leq 1 \mu M$, and for low stimulation by IP_3 , *i.e.* $[IP_3] \leq 0.24 \mu M$. ATP production decreases as $[AcCoA]$ is decreased except at the onset of oscillations, where a cusp in $[ATP]_c$ occurs (Figs. 2E and S1B). At this critical point, $[ATP]_c$ has become limiting for Ca^{2+} uptake by SERCAs and mitochondrial exchanges take over. This switch allows activation of TCA cycle enzymes by Ca^{2+} and locally rescues ATP production. Mitochondrial exchanges intensify as $[AcCoA]$ is further decreased. The larger Ca^{2+} efflux from mitochondria exerts a positive feedback on IP_3 R s which open more frequently, hence the decrease in oscillation period.

The efficiency of mitochondrial metabolism displays a maximum in the regime of Ca^{2+} spiking. The nonlinear ATP production (Fig. 2D) observed for different stimulation conditions in non-starving cells suggests variations in the output work of mitochondria and, possibly, in the thermodynamic efficiency of their metabolism. As confirmed computationally, the output nonconservative work (\bar{w}_{rout}) displays a minimum (corresponding to maximal *export* of energy from mitochondria) that coincides with the maximal $[ATP]_c$ in the kinetic simulations (Fig. 3A top and 3C bottom). On the other hand, both the non-conservative input work contributions (\bar{w}_{rin} and \bar{w}_{r2}) increase with $[IP_3]$ (almost monotonically until the end of the oscillatory regime), while the driving work (\bar{w}_{driv}) is always negligible compared to the total dissipation (Fig. 3A).

Importantly, the maximum in $[ATP]_c$ translates into a maximum in the efficiency of mitochondrial metabolism (Fig. 3C). Such maxima are not systematically observed when $[AcCoA]$ is varied at fixed $[IP_3]$ (Fig. S1A-B in SI Appendix). However, the increase in efficiency at the onset of the oscillatory regime is a robust feature that points to the stabilising effect of Ca^{2+} spikes on mitochondrial energetics.

Efficiency and total dissipation saturate at high stimulation of the Ca^{2+} signaling machinery. Like in other biological processes such as the migration of molecular motors along microtubules, kinetic proofreading or the regulation of circadian clocks (45), the system's efficiency is maximal at intermediate levels of dissipation, corresponding to a limited range of $[IP_3]$ (Fig. 3D). This finding indicates that overstimulation of the signaling machinery is counterproductive since it only increases dissipation (Fig. 3A bottom). By exploring the behavior of efficiency and total EPR at large $[IP_3]$, we observed a saturation effect leading to limiting values for the efficiency (≈ 0.236) and total dissipation ($\approx 5680 \text{ JL}^{-1} \text{ s}^{-1}$).

Interestingly, the dependency of efficiency on the total dissipation is highly nonlinear (Fig. 3D). Around the onset of oscillations (and for a limited range of dissipation rates), a given dissipation rate can be associated to different efficiencies, in which case the highest efficiency is always reached

for the highest Ca^{2+} spiking frequency, while the lowest efficiency corresponds to the steady-state regime. Reversely, different dissipative regimes can yield the same efficiency. In that case, steady-state regimes display the lowest EPR while the fast-spiking regimes are the more dissipative regimes. We hypothesize that in such instances, the selection of the dissipative regime could be guided by constraints imposed by the global energy budget of the cell.

Robustness of the efficiency-rescuing effect of Ca^{2+} oscillations. Our proposed mechanism for the maximum in efficiency relies on the dependence of the SERCA flux (J_{SERCA}) on the hydrolysis of ATP_c and on the resulting modulation of Ca^{2+} sequestration mechanisms. If Ca^{2+} homeostasis was ATP_c -independent, Ca^{2+} would always exert a positive feedback on the TCA cycle flux and the efficiency of metabolism would increase monotonically with the Ca^{2+} release from IP_3 R s. We validated this hypothesis by performing simulations with a modified SERCA flux that is uncoupled from ATP_c hydrolysis. The degradation of ATP_c then relies exclusively on other ATP_c -consuming processes mimicking cellular activity (Hyd reaction in Fig. 1A). As expected, the Ca^{2+} -enhanced ATP production by mitochondria is not restrained upon more intense stimulation by IP_3 (Fig. 4A). This uncoupling also disables the feedback of ATP production by mitochondria on Ca^{2+} oscillations: instead of decreasing, the spike period is barely changed as $[AcCoA]$ decreases (Fig. 4B).

In the uncoupled case, J_{SERCA} is not limited by the depletion of ATP_c and both removal mechanisms proceed synchronously, although Ca^{2+} uptake to the ER is predominant (Fig. 4C, green dotted curve). While the mitochondrial Ca^{2+} influx J_{UNI} slightly increases with J_{SERCA} , the Ca^{2+} -dependent currents of the TCA cycle, J_{IDH} and J_{KGDH} (Fig. 4C, purple dotted curves), are barely affected. Upon regulation by ATP_c , J_{SERCA} varies over a more restricted range, is on average smaller and proceeds with a slight phase shift with respect to J_{UNI} , which allows for a larger Ca^{2+} influx in mitochondria and a more intense activation of the TCA cycle enzymes (Fig. 4C solid curves). This mechanism supports the “efficiency-rescuing” role of mitochondrial buffering that is visible near the onset of oscillations in the coupled case (Figs. 3C and 4A bottom), while no such cusp-like transition is observed in the uncoupled case (Fig. 4A top).

We also explored the robustness of our results against perturbations in the uptake rate of SERCA pumps of the original model. We mimicked the inhibition of SERCA pumps by decreasing the limiting rate V_{max}^{SERCA} . Interestingly, the efficiency-dissipation relation displays the same features as in the non-inhibited case (Fig. 3F vs Fig. 3D). In the extreme case where oscillations disappear for large stimulation by IP_3 , the efficiency drops and reaches a plateau (Fig. 3E top).

Together, these results confirm that the cross-talk between Ca^{2+} signaling and mitochondrial energy metabolism is a major mechanism underlying the maximum in efficiency arising in the spiking regime, even when the amplitude of this coupling is reduced due to the inhibition of SERCA pumps.

Discussion

Here, we examined the impact of Ca^{2+} signaling on the efficiency of mitochondrial metabolism by using tools from the nonequilibrium thermodynamics of CRNs on a detailed

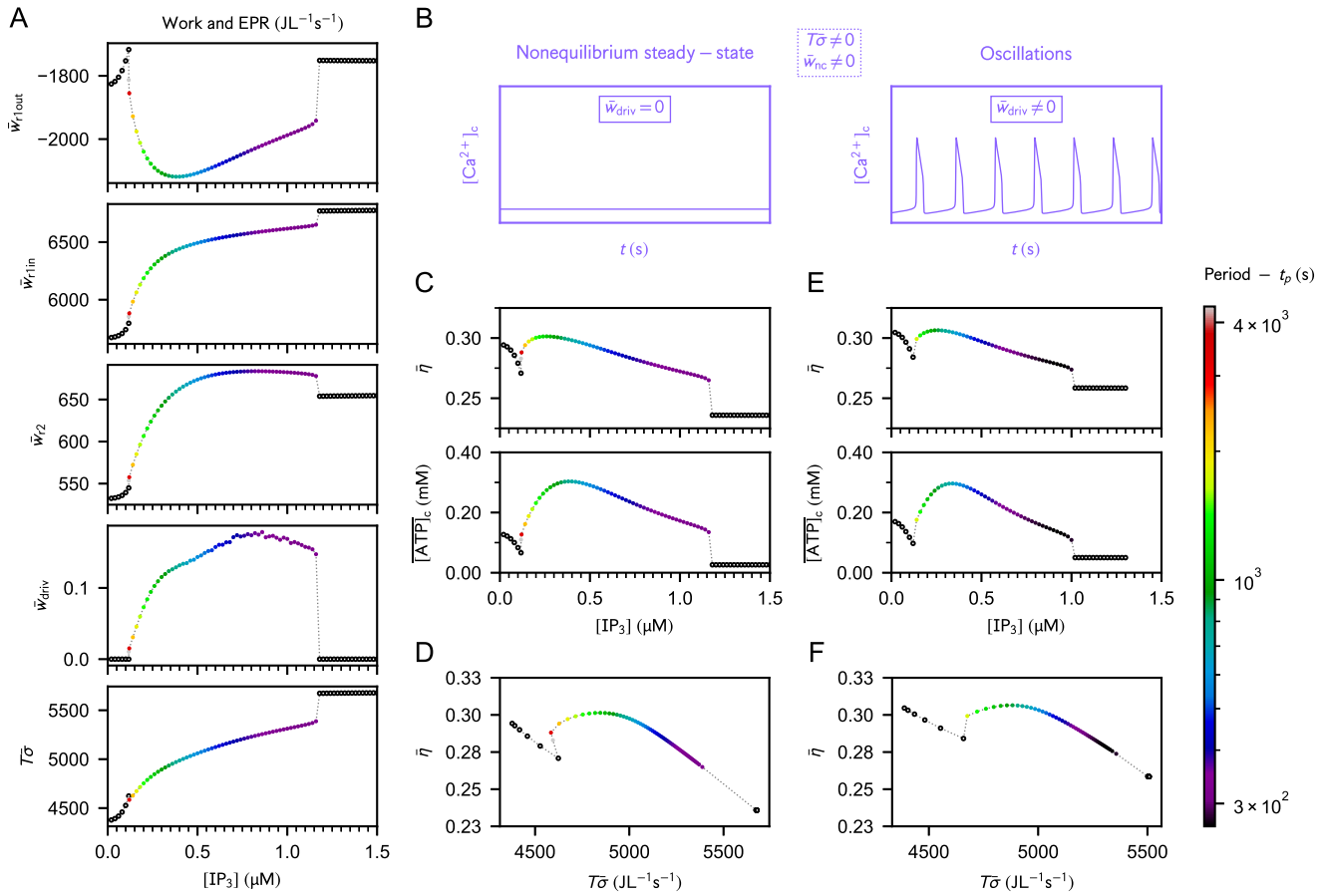


Fig. 3. Stimulating the Ca²⁺ signaling machinery impacts the dissipation and efficiency of mitochondrial metabolism via the Ca²⁺-metabolism cross-talk. (A) Nonconservative work contributions, driving work and dissipation for different [IP₃]. The driving work represents less than 0.01% of the EPR. At high stimulation, oscillations disappear in the favor of a nonequilibrium steady-state regime. (B) Expected work contributions in out-of-equilibrium conditions. (C) Efficiency and ATP_c concentration as a function of [IP₃]. (D) Efficiency as a function of the total dissipation for a range of [IP₃] extended up to 5 μM. (E-F) Plots corresponding to (C-D) for $V_{max}^{SERCA} = 0.08 \mu\text{M s}^{-1}$. Empty and filled dots correspond to steady-state or period-averaged quantities, respectively. Unless specified otherwise, parameter values are the same as in Fig. 2D.

and experimentally validated kinetic model of the Ca²⁺-metabolism cross-talk. Our results highlight that, despite a usually higher dissipation rate compared to steady-state regimes, Ca²⁺ oscillations can enhance the efficiency of mitochondrial metabolism. In particular, stimulation by IP₃ reduces the steady-state efficiency of metabolism but at the onset of oscillations the efficiency raises with a cusp-like transition and reaches a maximum of about 30% before decreasing again at higher stimulation. This value corresponds to the efficiency of the TCA cycle estimated in the absence of regulation with a non-equilibrium thermodynamic approach (16). Moreover, slow-spiking is less dissipative than fast-spiking. Thus, we hypothesize that, for a given cell state, there exists an optimal stimulation level leading to slow-spiking/low-dissipation oscillations which maximize the efficiency of metabolism during signaling. For higher stimulation, the Ca²⁺ signaling machinery then generates more dissipative regimes of gradually decreasing efficiency.

In the broader context of physical bioenergetics, energetic costs are usually assessed by evaluating the Gibbs free energy of reaction ($\Delta_r G$) dissipated or the equivalent number of ATP molecules produced/consumed along the processes of interest (8, 14, 15). However, such purely thermodynamic approaches do not account for reaction kinetics and thus cannot quantify

the rates of free energy transduction and dissipation. Significant efforts have been made in the direction of adding thermodynamic constraints in flux balance analysis of metabolic networks (46, 47). A few attempts have also been made to account for more complex kinetic effects such as enzyme saturation, leading to insights into the trade-offs between energy production and enzyme costs in glycolysis (12, 48, 49). Nevertheless, all these approaches rely on optimized nonequilibrium steady-states, which may not correspond to physiological conditions and cannot capture the energetic impact of time-dependent behaviors, such as the energy-rescuing effect of Ca²⁺ oscillations quantified here. Our novel approach overcomes these limitations, based on the rigorous thermodynamic analysis of a curated dynamical model.

Finally, a key mechanism of the Ca²⁺-mitochondria cross-talk and the metabolic efficiency management is the dynamical switch between SERCA and mitochondrial uptakes. Alterations in Ca²⁺ removal mechanisms due to mutations, generation of reactive oxygen species or remodeling of channel and pump expression are ubiquitous in pathological states such as mitochondrial (50) and neurodegenerative diseases (51, 52), cancer (53) or diabetes (54), and therapeutic strategies targeting Ca²⁺ homeostasis and signaling have started to emerge (55, 56). Overall, our methodology thus paves the way for a

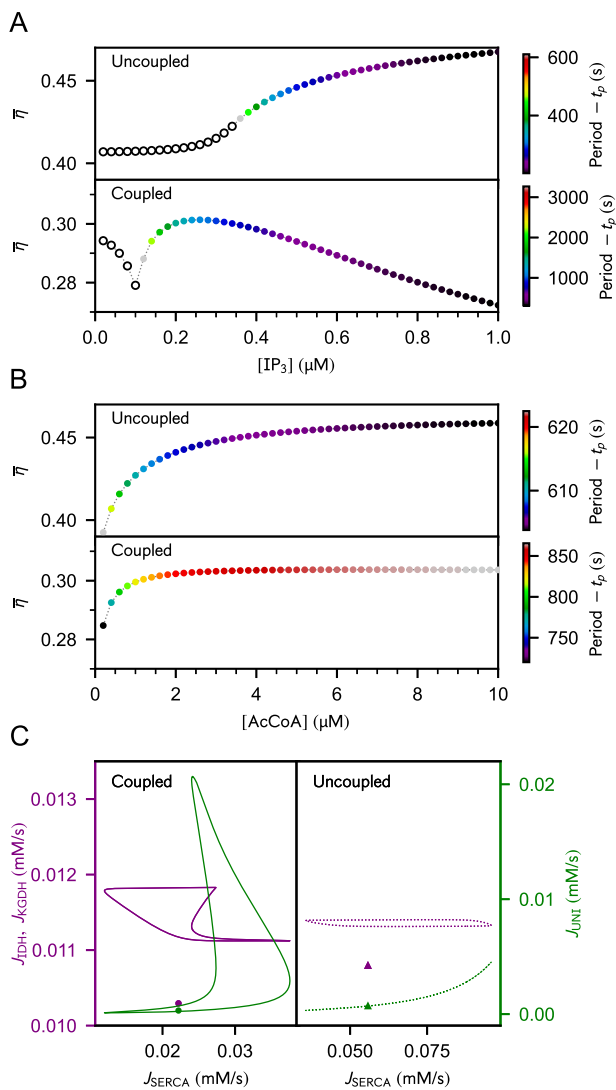


Fig. 4. Efficiency of mitochondrial metabolism regulated by Ca^{2+} signaling, Ca^{2+} sequestration fluxes and Ca^{2+} -dependent TCA cycle reaction fluxes, without and with the coupling of SERCA pumps to ATP_c hydrolysis. (A) Stimulating Ca^{2+} release by IP_3 R (that is, increasing $[IP_3]$) monotonically increases the efficiency in the uncoupled case, which strongly contrasts with the nonmonotonic dependency on $[IP_3]$ in the coupled case. While varying over different ranges, the period evolves according to the same trends in both cases. (B) Both systems display similar responses in their efficiency upon variations in $[AcCoA]$, but the oscillation period of the uncoupled system does not decrease – and is even slightly increasing – in stressing conditions corresponding to substrate depletion. As this observation is in contradiction with experimental evidence, the larger efficiencies reached in the uncoupled case are non physiological. Empty and filled dots correspond respectively to steady-state and oscillatory regimes – note the use of linear colorbar schemes for the period. (C) Phase portraits of Ca^{2+} -dependent TCA cycle currents (purple) and mitochondrial Ca^{2+} uptake (green), namely J_{IDH} , J_{KGDH} and J_{UNI} , vs. ER Ca^{2+} uptake, namely J_{SERCA} . Note that J_{IDH} and J_{KGDH} are indistinguishable. Symbols denote steady-state values. Triangles ($[IP_3] = 0.34 \mu M$) and dotted curves ($[IP_3] = 0.42 \mu M$) correspond to the uncoupled case, while circles ($[IP_3] = 0.10 \mu M$) and solid curves ($[IP_3] = 0.24 \mu M$) represent the coupled case. (A and C) $[AcCoA] = 1 \mu M$, (B) $[IP_3] = 0.36 \mu M$ and the other parameter values are the same as in Figs. 2–3.

more systematic characterization of the dynamical energetic impact of metabolism regulation, which could improve the current understanding of pathway selection mechanisms in

health and disease.

Materials and Methods

Model development, methodology and calculations are detailed in the SI Appendix, which is organized as follows: (1) Description of the kinetic model, (2) Concepts of biothermodynamics and (3) Nonequilibrium thermodynamics analysis. A systematic description of the nonequilibrium thermodynamics of CRNs can be found in refs. (33, 36). This description can be applied to effective coarse-grained fluxes (34, 35) such as the ones we used to characterize the enzyme-catalysed processes of our system. The chemical reactions incorporated in the model are listed in Table S1 and the corresponding fluxes and forces are given in Tables S2 and S3, respectively. Lastly, the reference simulation parameters and a short description of their physical meaning can be found in Table S4.

ACKNOWLEDGMENTS. VV is funded by the Complex Living Systems Initiative at the University of Luxembourg. FA and ME are funded by the Luxembourg National Research Fund, grant ChemComplex (C21/MS/16356329). GF is funded by the European Union – NextGenerationEU – and by the program STARS@UNIPD with project "ThermoComplex". FA, AS and ME acknowledge financial support of the Institute for Advanced Studies of the University of Luxembourg through an Audacity Grant (IDAE-2020).

1. DG Nicholls, SJ Ferguson, *Bioenergetics 2*. (Academic Press, San Diego), (1992).
2. F Calisto, FM Sousa, FV Sena, PN Refojo, MM Pereira, Mechanisms of Energy Transduction by Charge Translocating Membrane Proteins. *Chem. Rev.* **121** (2021) Publisher: American Chemical Society.
3. MC Berman, Slippage and uncoupling in P-type cation pumps; implications for energy transduction mechanisms and regulation of metabolism. *BBA* **1513**, 95–121 (2001).
4. P Gräber, G Milazzo, *Bioenergetics*, Bioelectrochemistry: Principles and Practice. (Birkhäuser, Basel), (1997).
5. JM Rubi, M Nasprea, S Kjelstrup, D Bedeaux, Energy Transduction in Biological Systems: A Mesoscopic Non-Equilibrium Thermodynamics Perspective. *J. Non-Equilib. Thermodyn.* **32**, 351–378 (2007).
6. TL Hill, *Free Energy Transduction in Biology: The Steady-State Kinetic and Thermodynamic Formalism*. (Academic Press, New York), (2012).
7. M Wikström, R Springett, Thermodynamic efficiency, reversibility, and degree of coupling in energy conservation by the mitochondrial respiratory chain. *Commun Biol* **3**, 1–9 (2020).
8. X Yang, et al., Physical bioenergetics: Energy fluxes, budgets, and constraints in cells. *PNAS* **118** (2021).
9. J Estrada, F Wong, A DePace, J Gunawardena, Information Integration and Energy Expenditure in Gene Regulation. *Cell* **166**, 234–244 (2016).
10. P Sartori, S Pigolotti, Thermodynamics of Error Correction. *Phys. Rev. X* **5**, 041039 (2015).
11. P Goloubinoff, AS Sassi, B Fauvet, A Barducci, P De Los Rios, Chaperones convert the energy from ATP into the nonequilibrium stabilization of native proteins. *Nat. Chem. Biol.* **14**, 388–395 (2018).
12. A Flamholz, E Noor, A Bar-Even, W Liebermeister, R Milo, Glycolytic strategy as a tradeoff between energy yield and protein cost. *Proc. Natl. Acad. Sci. USA* **110**, 10039–10044 (2013).
13. JMR Parrondo, JM Horowitz, T Sagawa, Thermodynamics of information. *Nat. Phys* **11**, 131–139 (2015).
14. Y Cao, H Wang, Q Ouyang, Y Tu, The free-energy cost of accurate biochemical oscillations. *Nat. Phys.* **11**, 772–778 (2015).
15. J Rodenfels, KM Neugebauer, J Howard, Heat Oscillations Driven by the Embryonic Cell Cycle Reveal the Energetic Costs of Signaling. *Dev. Cell* **48**, 646–658.e6 (2019).
16. A Wachtel, R Rao, M Esposito, Free-energy transduction in chemical reaction networks: From enzymes to metabolism. *J. Chem. Phys.* **157**, 024109 (2022).
17. JG McCormack, Characterization of the effects of Ca^{2+} on the intramitochondrial Ca^{2+} -sensitive enzymes from rat liver and within intact rat liver mitochondria. *Biochem. J.* **231**, 581–595 (1985).
18. G Hajnóczky, LD Robb-Gaspers, MB Seitz, AP Thomas, Decoding of cytosolic calcium oscillations in the mitochondria. *Cell* **82**, 415–424 (1995).
19. EJ Griffiths, GA Rutter, Mitochondrial calcium as a key regulator of mitochondrial ATP production in mammalian cells. *Biochimica et Biophys. Acta (BBA) - Bioenerg.* **1787**, 1324–1333 (2009).
20. RM Denton, Regulation of mitochondrial dehydrogenases by calcium ions. *BBA* **1787**, 1309–1316 (2009).
21. MJ Berridge, MD Bootman, P Lipp, Calcium—a life and death signal. *Nature* **395**, 645–648 (1998).
22. S Dudycha, M.S. Dissertation (Johns Hopkins University) (2000).
23. G Magnus, J Keizer, Minimal model of beta-cell mitochondrial Ca^{2+} handling. *A. J. Physiol.* **273**, C717–733 (1997).
24. G Magnus, J Keizer, Model of beta-cell mitochondrial calcium handling and electrical activity. I. Cytoplasmic variables. *Am. J. Physiol.* **274**, C1158–1173 (1998).

25. G Magnus, J Keizer, Model of beta-cell mitochondrial calcium handling and electrical activity. II. Mitochondrial variables. *Am J Physiol* **274**, C1174–1184 (1998).
26. N Berndt, O Kann, HG Holzhütter, Physiology-based kinetic modeling of neuronal energy metabolism unravels the molecular basis of NAD(P)H fluorescence transients. *J. Cereb. Blood Flow Metab.* **35**, 1494–1506 (2015).
27. N Komin, M Moein, MH Ellisman, A Skupin, Multiscale Modeling Indicates That Temperature Dependent $[Ca^{2+}]_i$ Spiking in Astrocytes Is Quantitatively Consistent with Modulated SERCA Activity. *Neural Plast.* **2015**, 683490 (2015).
28. B Wacquier, L Combettes, GT Van Nhieu, G Dupont, Interplay Between Intracellular Ca^{2+} Oscillations and Ca^{2+} -stimulated Mitochondrial Metabolism. *Sci. Rep.* **6**, 19316 (2016).
29. S Cortassa, MA Aon, E Marbán, RL Winslow, B O'Rourke, An integrated model of cardiac mitochondrial energy metabolism and calcium dynamics. *Biophys. J.* **84**, 2734–2755 (2003).
30. R Bertram, M Gram Pedersen, DS Luciani, A Sherman, A simplified model for mitochondrial ATP production. *J. Theor. Biol.* **243**, 575–586 (2006).
31. AC Wei, M Aon, B O'Rourke, R Winslow, S Cortassa, Mitochondrial Energetics, pH Regulation, and Ion Dynamics: A Computational-Experimental Approach. *Biophys. J.* **100**, 2894–2903 (2011).
32. R Rao, M Esposito, Nonequilibrium Thermodynamics of Chemical Reaction Networks: Wisdom from Stochastic Thermodynamics. *Phys. Rev. X* **6**, 041064 (2016).
33. R Rao, M Esposito, Conservation laws and work fluctuation relations in chemical reaction networks. *J. Chem. Phys.* **149**, 245101 (2018).
34. A Wachtel, R Rao, M Esposito, Thermodynamically consistent coarse graining of biocatalysts beyond Michaelis–Menten. *New J. Phys.* **20**, 042002 (2018).
35. F Avanzini, G Falasco, M Esposito, Thermodynamics of non-elementary chemical reaction networks. *New J. Phys.* **22**, 093040 (2020).
36. F Avanzini, E Penocchio, G Falasco, M Esposito, Nonequilibrium thermodynamics of non-ideal chemical reaction networks. *J. Chem. Phys.* **154**, 094114 (2021).
37. F Avanzini, M Esposito, Thermodynamics of concentration vs flux control in chemical reaction networks. *J. Chem. Phys.* **156**, 014116 (2022).
38. NM Woods, KSR Cuthbertson, PH Cobbold, Repetitive transient rises in cytoplasmic free calcium in hormone-stimulated hepatocytes. *Nature* **319**, 600 (1986).
39. M Falcke, Reading the patterns in living cells—the physics of Ca^{2+} signaling. *Adv. Phys.* **53**, 255–440 (2004).
40. G Dupont, L Combettes, L Leybaert, Calcium dynamics: spatio-temporal organization from the subcellular to the organ level. *Int. Rev. Cytol.* **261**, 193–245 (2007).
41. K Thurley, et al., Reliable Encoding of Stimulus Intensities Within Random Sequences of Intracellular Ca^{2+} Spikes. *Sci. Signal.* **7**, ra59–ra59 (2014).
42. M Moein, PhD Thesis (University of Luxembourg) (2017).
43. LS Jouaville, F Ichas, EL Holmuhamedov, P Camacho, JD Lechleiter, Synchronization of calcium waves by mitochondrial substrates in *Xenopus laevis* oocytes. *Nature* **377**, 438–441 (1995).
44. DA Eisner, M Valdeolmillos, A study of intracellular calcium oscillations in sheep cardiac Purkinje fibres measured at the single cell level. *J. Physiol.* **372**, 539–556 (1986).
45. M Baiesi, C Maes, Life efficiency does not always increase with the dissipation rate. *J. Phys. Commun.* **2**, 045017 (2018).
46. DA Beard, Sd Liang, H Qian, Energy Balance for Analysis of Complex Metabolic Networks. *Biophys. J.* **83**, 79–86 (2002).
47. B Niebel, S Leupold, M Heinemann, An upper limit on Gibbs energy dissipation governs cellular metabolism. *Nat. Metab.* **1**, 125–132 (2019).
48. E Noor, A Flamholz, W Liebermeister, A Bar-Even, R Milo, A note on the kinetics of enzyme action: A decomposition that highlights thermodynamic effects. *FEBS Lett.* **587**, 2772–2777 (2013).
49. Al Stettner, D Segrè, The cost of efficiency in energy metabolism. *Proc. Natl. Acad. Sci. U.S.A.* **110**, 9629–9630 (2013).
50. HJ Visch, et al., Ca^{2+} -mobilizing agonists increase mitochondrial ATP production to accelerate cytosolic Ca^{2+} removal: aberrations in human complex I deficiency. *Am. J. Physiol. Physiol.* **291**, C308–C316 (2006).
51. F Celsi, et al., Mitochondria, calcium and cell death: A deadly triad in neurodegeneration. *Biochim. Biophys. Acta* **1787**, 335–344 (2009).
52. R Filadi, P Pizzo, Mitochondrial calcium handling and neurodegeneration: when a good signal goes wrong. *Curr. Opin. Physiol.* **17**, 224–233 (2020).
53. GR Monteith, N Prevarskaya, SJ Roberts-Thomson, The calcium–cancer signalling nexus. *Nat. Rev. Cancer* **17**, 373–380 (2017).
54. A Guerrero-Hernandez, A Verkhratsky, Calcium signalling in diabetes. *Cell Calcium* **56**, 297–301 (2014).
55. C Giorgi, et al., Mitochondrial calcium homeostasis as potential target for mitochondrial medicine. *Mitochondrion* **12**, 77–85 (2012).
56. C Dejos, D Gkika, AR Cantelmo, The Two-Way Relationship Between Calcium and Metabolism in Cancer. *Front. Cell Dev. Biol.* **8**, 573747 (2020).